Calculation of 10g average SAR via inversion of the heat equation using MRI Thermometry and Thermal Property Measurements

Leeor Alon[1,2], Gene Cho[1,2], Leslie F. Greengard[3], Ricardo Otazo[1,2], Daniel K. Sodickson[1,2], and Cem M. Deniz[1,2]

[1]*Department of Radiology, Bernard and Irene Schwartz Center for Biomedical Imaging, New York University School of Medicine, New York, NY, United States,* [2]*Sackler Institute of Graduate Biomedical Sciences, New York University School of Medicine, New York, NY, United States,* [3]*Courant Institute of Mathematical Sciences, New York University, NY, United States*

INTRODUCTION: In MRI, RF energy deposition inside the body is regulated via whole body and local SAR metrics [1]. Experimental studies have shown that measurement of temperature change (ΔT) using MRI can be used to quantify RF antenna exposure [2,3]. In order to ensure RF safety regulations using SAR, ΔT needs to be converted to 10g average SAR. During experiments, RF heating duration needs to be kept short for capturing the initial slope of the temperature increase. In practice however, the E fields produced by the antenna, the maximum power capabilities of the RF amplifiers, and conductivity of the phantom can be limiting factors, requiring longer RF heating duration for accurate MR thermometry. In such cases, heat diffusion in the phantom cannot be ignored and the conversion of ΔT to 10g average SAR becomes non-trivial (illustrated in Fig 2). In this work, we take advantage of high-resolution MR temperature mapping measurements alongside phantom physical thermal property measurements to invert the heat equation using sparsity constraints and compute the 10g average SAR distribution. Heat equation inversion results are validated using Electromagnetic (EM) field simulation and MR experiments, enabling a generalized experimental accurate computation of 10g average SAR from MR thermometry measurements in phantoms.

THEORY: The heat equation with SAR as the source term inside a non-perfuse, homogeneous medium is expressed as follows:

$$\rho C \frac{dT}{dt} = \nabla \cdot (k \nabla T) + SAR\rho \quad (1).$$

where ρ, C, k, and SAR are the tissue density (kg/m^3), heat capacity (J/kg/C), thermal conductivity (W/m/C), and SAR (W/kg) is the driving force for temperature rise defined as: $SAR = \frac{\sigma |E|^2}{2\rho}$. Where **E** is the induced electric field (V/m), and σ is the electrical conductivity (S/m). When the heating duration is short, Eq. (1) can be simplified to: $SAR = C\frac{\Delta T}{\Delta t}$ (2) where Δt is the RF heating time-interval. In order to account for the heat diffusion, a finite difference approximation of the heat equation was used in polynomial form such that [4]:

$$T_N = (1+L)^N T_1 + \sum_{i=0}^{N-2} (1+L)^i f \quad (3).$$

where f is the source term defined as: $f = \Delta t * SAR * C^{-1}$, T_1 and T_N are the initial and final temperature of the sample, respectively, and L is a linear Laplace operator defined as: $L = \Delta t * \frac{k}{\rho C} * \nabla^2$. Since all the terms in Eq. (3), except f, are measurable quantities (k and C can be measured using a thermal probe, and $\Delta T = T_N - T_1$ using MR), the solution to this problem can be written in a linear matrix notation. f, which is sparsely represented, is calculated using the following l_1 norm weighted least squares minimization, which has been shown to be robust with respect to noise for sparse representations [5]:

$$argmin_f \{ \|Af - b\|_2 + \lambda \|f\|_1 \quad (4)$$

where $b = T_N - (1+L)^{N-1} T_1$, $A = \sum_{i=0}^{N-2} (1+L)^i$, and λ is the regularization parameter.

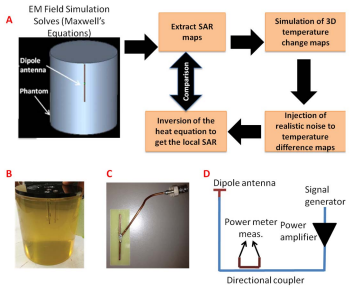

Figure 1. **A**. Phantom-dipole antenna setup and flow chart of the process used for the solution of the inverse heat problem. **B-** Gel phantom used in MR temperature mapping experiments. The phantom properties were as follows: ρ=1272 (kg/m^3), C=3543 (J/kg·°C) and k=0.457 (W/m·°C). **C-** Dipole antenna used in the MR experiments. **D-** Schematic of the experiment setup used to drive the dipole antenna.

METHODS: A cylindrical acrylic former [Fig. 1A] with a diameter of 10.2 cm and a height of 11cm was filled with gelatin. EM field simulations were performed on the dipole antenna, to obtain the SAR distribution induced by the dipole antenna inside the phantom and validate that the heat equation inversion problem can be solved accurately. Commercial software (Microwave Studio; CST, MA, USA) using finite integration technique (FIT) was used for the simulations. The parameters used in the FIT calculations were: 2.7 mm isotropic cell size, mesh dimensions 84 x 83 x 83, feeding with a voltage source operating at 1.96 GHz, generating a net input power of 0.65W. The simulated SAR distribution was used along with the thermal properties of the phantom to model the temperature distribution in the phantom numerically by solving the Heat equation (Eq. 1) as result of 6.5 minutes of heating [6]. Gaussian noise (similar in mean and standard deviation of the MR temperature mapping) with standard deviation of 0.1°C was added to the simulated temperature maps. Inversion of the heat equation was then conducted using Eq. 4 with the regularization parameter, λ=1.5. The 10g average SAR was calculated from the point SAR and compared with the true 10g average SAR distribution that was directly computed in EM field simulation. A flow chart of the procedure is shown in Fig. 1A. For the experiments, a half wavelength (λ/2) dipole antenna (Fig. 1C) was constructed to operate at 1.96GHz and matched for maximum efficiency with S11 < -15 dB. The schematic of the experimental setup used is shown in Fig. 1D. During the RF heating period, the antenna was operated in continuous wave mode for 6.5 minutes and net transmitted RF power was monitored using a directional coupler (Agilent, 778D) and a power sensor (NRP-Z11, Rhode & Schwarz). RF heating was detected using a 3T MR scanner and head and neck coil (Siemens, Germany) with 20 receive elements. Multi-slice, interleaved, spoiled gradient-echo (GRE) phase images of the phantom before and after RF heating were measured to compute ΔT using the proton resonance frequency (PRF) shift method [7]. The following sequence parameters where used: TR= 244 ms, TE = 17 ms, voxel size = 2.7x2.7x5 mm^3, slices = 11 and acquisition time = 31s. The temperature difference map and the thermal properties of the phantom, measured using a thermal property analyzer (KD2 Pro, WA, USA), were used to invert the heat equation and compute the 10g average SAR. The 10g average SAR maps calculated and plotted using the over-simplified Eq. (2) and the new method shown in Eq. (4).

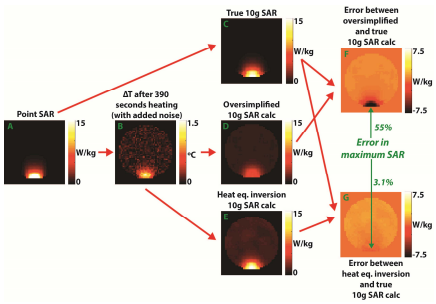

Figure 2 **A**- simulated point SAR. **B**- simulated ΔT map after 390 seconds of heating by a dipole antenna outputting 0.65W at 1.96GHz. **C-** true 10g average SAR calculated from spatial averaging of the point SAR distribution. **D-** 10g average SAR map calculated by over simplifying the temperature change (B) to yield point SAR (using Eq. 2)**. E**- 10g average SAR map calculated by inverting the heat equation (Eq. 1) using the ΔT map and measured thermal properties of the phantom. **F**- error map between the oversimplified and true 10g average SAR calculation. Error at the maximum SAR location was 8.8W, which is 55% of the maximum true 10g average SAR. **G**- error map between the heat equation inversion and true 10g average SAR reconstructions. Error at the maximum SAR location was 0.8W, which is 3.1% of the maximum true 10g average SAR.

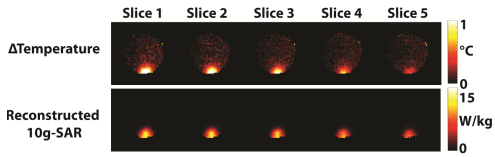

Figure 3 Experimentally measured ΔT maps and reconstructed 10g average SAR maps at 5 slices inside the phantom.

RESULTS: Fig 2 illustrates the SAR underestimation of simple scaling of the temperature change to quantify 10g averages SAR. Fig. 3A shows an EM field simulation comparison between the reconstructed and true 10g average SAR results for five slices in the middle of the phantom. The maximum error between the reconstructed and true 10g average SAR distributions over the entire volume of the phantom was 0.8 W/kg. Simulation results show that the maximum 10g average SAR can be reconstructed within 3.1%, whereas the simplified method underestimated SAR by more than 55%. Experimental 10g average SAR results are shown in Fig. 3B, where temperature maps of RF heating from a dipole antenna positioned inside the MR scanner room were used in solving the inverse heat problem.

CONCLUSION: In summary, a generalized method for experimentally computing 10g average SAR is presented in this work. High resolution MRI temperature mapping alongside thermal property measurements of a phantom enabled conversion ΔT to 10g average SAR to be used as metric for safety evaluation of RF emitting devices.

REFERENCES: [1] IEC, 60601-2-33, 2010. [2] C.M. Deniz, et al., ISMRM, 2013, p. 4424. [3] L. Alon, et al., ISMRM, 2013, p. 3593. [4] L. Yan, et al., International Journal for Numerical Methods in Biomedical Engineering, vol. 26, pp. 597-608, 2010. [5] E. J. Candes et al., IEEE Transactions on Information Theory, vol. 52, pp. 5406-5425, 2006. [6] C. M. Collins et al., JMRI, vol. 19, pp. 650-6, May 2004. [7] V. Rieke et al., JMRI, vol. 27, pp. 376-90, Feb 2008.